Structural investigations on $PbO–Sb_2O_3–B_2O_3$:CoO glass ceramics by means of spectroscopic and dielectric studies

2009 J. Phys.: Condens. Matter 21 245104

(http://iopscience.iop.org/0953-8984/21/24/245104)

J. Phys.: Condens. Matter **21** (2009) 245104 (16pp) doi:10.1088/0953-8984/21/24/245104

Structural investigations on $PbO–Sb_2O_3–B_2O_3$:CoO glass ceramics by means of spectroscopic and dielectric studies

T Satyanarayana[1], I V Kityk[2,3], M Piasecki[4], P Bragiel[4], M G Brik[5], Y Gandhi[1] and N Veeraiah[1,6]

[1] Department of Physics, Acharya Nagarjuna University-Nuzvid Campus, Nuzvid 521 201, AP, India
[2] Electrical Engineering Department, Technological University of Czesdothcowa, Aleja Armii Krajowej 17/19, PL-42-201 Czestochowa, Poland
[3] Chemical Department, Silesian Technological University, ulica Strzody 9, PL-44-100 Gliwice, Poland
[4] Institute of Physics, J Dlugosz University Czestochowa, Aleja Armii Krajowej 13/15, 42-200 Czestochowa, Poland
[5] Institute of Physics, University of Tartu, Riia 142, Tartu 51014, Estonia

E-mail: nvr8@rediffmail.com

Received 16 January 2009, in final form 13 April 2009
Published 12 May 2009
Online at stacks.iop.org/JPhysCM/21/245104

Abstract

$PbO–Sb_2O_3–B_2O_3$ glasses mixed with different concentrations of CoO (ranging from 0 to 2.0 mol%) were crystallized. The samples were characterized by x-ray diffraction, scanning electron microscopy and differential scanning calorimetric techniques. The x-ray diffraction and scanning electron microscopic studies have revealed the presence of $CoSb_2O_6$, $Co_{2.33}Sb_{0.67}O_4$, $Pb_5Sb_2O_8$, $Pb_3(SbO_4)_2$, PbB_4O_7 and Co_3O_4 crystalline phases in these samples. The DSC studies have indicated the spreading of the crystallization from the inside to the surface of the samples as the concentration of the crystallizing agent is increased. The IR and Raman spectroscopic studies have pointed out the existence of conventional BO_3, BO_4, SbO_4 and also Co^{III}–O structural units in the glass ceramic samples. These studies have further indicated the decreasing concentration of symmetrical structural vibrational groups with increase in the concentration of CoO. The results of various studies, namely dielectric properties over a range of frequency and temperature, photo-induced birefringence, optical absorption, fluorescence and magnetic susceptibility at room temperature of $PbO–Sb_2O_3–B_2O_3$:CoO glass ceramics, have also been reported. The variations observed as a function of the concentration of crystallizing agent in all these properties have been analyzed in the light of different oxidation states and environments of cobalt ions in the glass ceramic network.

(Some figures in this article are in colour only in the electronic version)

1. Introduction

Cobalt ions are being extensively investigated in several commercial silica-based glasses, glass ceramics and other crystalline dielectric materials [1–4]. The glasses and glass ceramics containing cobalt ions are good candidates for nonlinear optical absorbers, needed for passive modulations of laser beams [5]. These materials are also considered as useful materials for Q-switching devices [6, 7], in view of the fact that they exhibit strong luminescence in the visible and near-infrared regions. In glasses, cobalt ions exist in two stable ionic states, namely Co^{2+} and Co^{3+}. Co^{2+} ions create

[6] Author to whom any correspondence should be addressed.

color centers with absorption bands in the visible and NIR regions [8] and produce blue and pink glasses. The color of the glass depends on the Co^{2+} content, its specific coordination (tetrahedral or octahedral), composition and basicity of the glass. Though a reasonably large number of recent studies on the environment of cobalt ions by means of spectroscopic studies are available, most of them are restricted mainly to silicate glasses and glass ceramics. The structural probing of cobalt ions, especially in heavy metal oxide-based glass ceramics like lead antimony oxide, is highly desirable since these glasses have got potential applications in nonlinear optical devices (such as ultrafast optical switches, power limiters and broadband optical amplifiers operating around 1.5 μm) [9, 10]. Further, Sb_2O_3-based glass ceramics possess high refractive index and are transparent to the far-infrared wavelengths [11]. Antimony oxide participates in the glass network with SbO_3 structural units and can be viewed as tetrahedra with the oxygens situated at three corners and the lone pair of electrons of antimony (Sb^{3+}) at the fourth corner localized in the third equatorial direction of the Sb atom. The deformability of this pair probably could make these glass ceramics exhibit nonlinear optical susceptibility described by third rank polar tensors [11]. These factors favor different optically polarized effects. Antimony ions may also exist in the Sb^{5+} state, participate in the formation of a glass network with $Sb^{5+}O_4$ structural units and may form linkages with BO_4 structural units in the $PbO–Sb_2O_3–B_2O_3$ glass ceramic network and influence the nonlinear optical effects of these glass ceramics to a large extent.

In general, glass ceramic materials are expected to have several advantages like good mechanical, electrical and thermal properties, high chemical durability and low coefficient of thermal expansion with no crack growth inside. Hence, considerable interest is attached in this connection to the studies on crystallization of the glass materials and its bearing on the physical properties. If care is taken that the average diameter of various crystalline grains produced in the glass ceramics is sufficiently far away from the wavelengths of the visible and NIR spectral regions, these samples retain transparency even after crystallization. Further, the glass ceramic materials are more stable against the laser pulses when compared with the amorphous materials. Catalysts generally used for controlling crystallization processes, giving rise to enormous numbers of nucleation centers in the original glass, are gold, silver, platinum or the oxides of transition metals like Ti, Cr, Mn, Ce, V, Fe, Co, Ni, Zr, etc, or certain sulfides or fluorides of heavy transition metals. However, the crystallization of lead antimony oxide-based glasses with CoO is an added advantage for exhibiting high nonlinear optical effects by these materials since the electron phonon interaction between the glass ceramic network and the cobalt ions is reported to be very strong with pronounced anharmonic effects [12].

Thus the present investigation is aimed at the synthesis of $PbO–Sb_2O_3–B_2O_3$ glass ceramics with different concentrations of CoO as nucleating agent, at characterizing them by a variety of techniques, namely XRD, SEM, DSC and energy-dispersive spectra (EDS), and examining the suitability of these

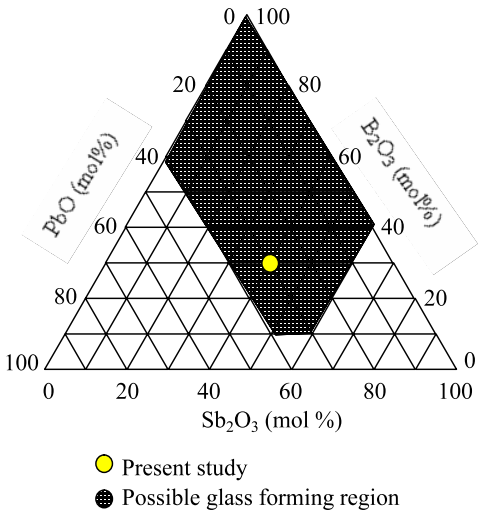

Figure 1. Approximate glass-forming region of $PbO–Sb_2O_3–B_2O_3$ glass system.

materials in optically operated devices (based prevailingly on the optical Kerr effect) by investigating their physical properties. The studies taken up are spectroscopic properties (optical absorption, Raman, IR and photoluminescence), magnetic and dielectric properties and the corresponding photo-induced birefringence (PIB) in the nanosecond time region. By studying photo-induced birefringence we deal not only with the pure optical Kerr effect, but also with different photo-thermal and photo-bleaching factors that contribute to birefringence.

The contents of the paper are as follows: section 1 presents the technology of sample preparation and the details of experimental techniques adopted for sample characterization. In section 2 the results of characterization studies, namely electron microscopy, x-ray diffraction, EDS analysis and DSC/TG, are presented. Section 3 is devoted to the presentation of the studies on physical properties including photo-induced birefringence. In section 4, the principal influence of cobalt ion and its environment (tetrahedral, octahedral) on physical properties is presented.

2. Experimental methods

Within the possible glass-forming region (figure 1) of the $PbO–Sb_2O_3–B_2O_3$ system, a particular composition 30 PbO–40 Sb_2O_3–30 B_2O_3 is chosen for the present study. The crystallizing agent CoO is varied from 0 to 2.0 mol% in this glass matrix. The detailed compositions are as follows:

C_0: 30 PbO–40 Sb_2O_3–30 B_2O_3

C_2: 29.8 PbO–40 Sb_2O_3–30 B_2O_3:0.2 CoO

C_4: 29.6 PbO–40 Sb_2O_3–30 B_2O_3:0.4 CoO

C_6: 29.4 PbO–40 Sb_2O_3–30 B_2O_3:0.6 CoO

C_8: 29.2 PbO–40 Sb_2O_3–30 B_2O_3:0.8 CoO

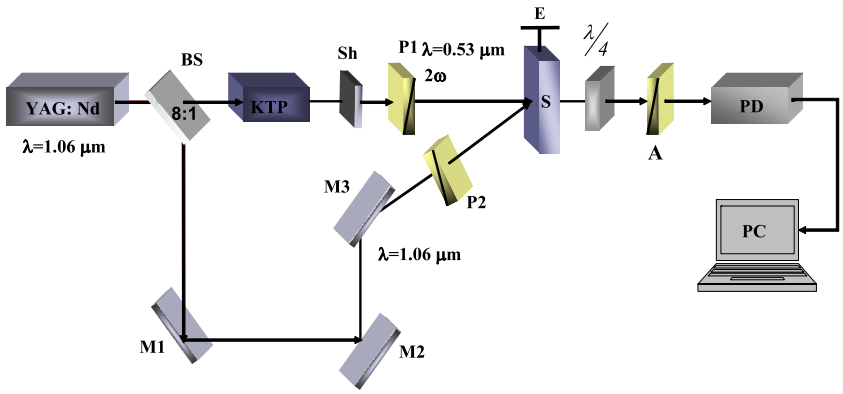

Figure 2. Principal experimental set-up used for photo-induced birefringence measurement.

C_{10}: 29.0 PbO–40 Sb_2O_3–30 B_2O_3:1.0 CoO

C_{15}: 28.5 PbO–40 Sb_2O_3–30 B_2O_3:1.5 CoO

C_{20}: 28.0 PbO–40 Sb_2O_3–30 B_2O_3:2.0 CoO.

Analytical grade reagents of Sb_2O_3, H_3BO_3, PbO and CoO powders in appropriate amounts (all in mol%) were thoroughly mixed in an agate mortar and melted in a platinum crucible in the temperature range of 1000 to 1050 °C in a PID temperature-controlled furnace for about 1 h. The resultant bubble-free melt was then poured in a brass mold and subsequently annealed at 300 °C. The glass specimens with various concentrations of CoO were heat-treated in a furnace at 500 °C for 6 h. An automatically controlled furnace was used to keep the temperature at the desired level. After the heat treatment in the furnace at a specified temperature, the samples were cooled in air to room temperature. The samples prepared were ground and optically polished to the dimensions of 1 cm × 1 cm × 0.2 cm. The crystalline phases in the glass ceramic samples were identified using a Rigaku D/Max ULTIMA III x-ray diffractometer with Cu Kα radiation. Scanning electron microscopy studies were also carried out on these samples to observe the crystallinity using a Hitachi S-3400N scanning electron microscope. Differential thermal analysis was carried out by a Netzsch Simultaneous DSC/TG Thermal Analyzer STA409C with 32-bit controller to determine the glass transition temperature and crystalline peaks. A high temperature furnace together with a sample carrier suitable for C_p measurements and Al_2O_3 crucibles were used. The apparatus was calibrated both for temperature and for sensitivity with melting temperatures and melting enthalpies of the pure metals: Ga, In, Sn, Zn, Al, Ag, Au. All the recordings were carried out in argon (5N) atmosphere to prevent samples from oxidation. Heating rate was 10 °C min^{-1} in the temperature range 32–1300 °C. The density of the glass ceramics was determined to an accuracy of (±0.0001) by the standard principle of Archimedes' using *o*-xylene (99.99% pure) as the buoyant liquid. The mass of the samples was measured to an accuracy of 0.1 mg using an Ohaus digital balance Model AR2140 for evaluating the density. Infrared transmission spectra were recorded on a JASCO-FT/IR-5300 spectrophotometer up to a resolution of 0.1 cm^{-1} in the spectral range 400–2000 cm^{-1} using potassium bromide pellets (300 mg) containing a pulverized sample (1.5 mg). These pellets were pressed in a vacuum die at ∼680 MPa. The Raman spectra of this glass ceramics were recorded with an NIR excitation line (1064 nm) using a Bio-Rad spectrometer FTS 175C equipped with an FT Raman supplementary accessory working in a backscattering geometry system.

The optical absorption spectra of the glass ceramics were recorded with a spectral resolution of 0.1 at room temperature in the spectral wavelength range covering 300–1800 nm using a JASCO Model V-670 UV–vis–NIR spectrophotometer. The luminescence spectra of the samples were recorded at room temperature on a Photon Technology International fluorescence spectrophotometer. Magnetic susceptibility measurements were also carried out on these samples by Guoy's method using fine powders. The photo-induced birefringence (PIB) of the glass ceramics was measured using the standard nanosecond (ns) photo-induced technique (figure 2). An Nd:YAG laser operated at 10 Hz with a pulse duration of 10 ns was used as the fundamental laser light source. The fundamental laser beam was split into two beams by a beamsplitter with the intensity ratio 8:1. The strong beam acts as the pump one and the weak one as the probe. The two beams were adjusted to be almost parallel and then focused by a convex lens to overlap spatially inside the glass sample. After transmission through the specimen, the pump beam was blocked by a chopper, while the probe beam passed through a polarizer and phase inverter plate, which is an element of the Senarmont schema. After the rotation of the output signal, polarization was determined to evaluate the photo-induced birefringence. The photo-inducing 7 ns 1064 nm Nd:YAG laser was incident on the sample at an angle of about 5°–7° with respect to the surface normal. The photo-inducing UV laser beam and the probing laser beams were temporary synchronized. Varying successively the intensity of the photo-inducing beam power density, we have operated by pumping power density. A brief sketch of the (PIB) measurements is given in figure 2. The details of measurements of dielectrics were similar to those reported in our earlier papers [13, 14].

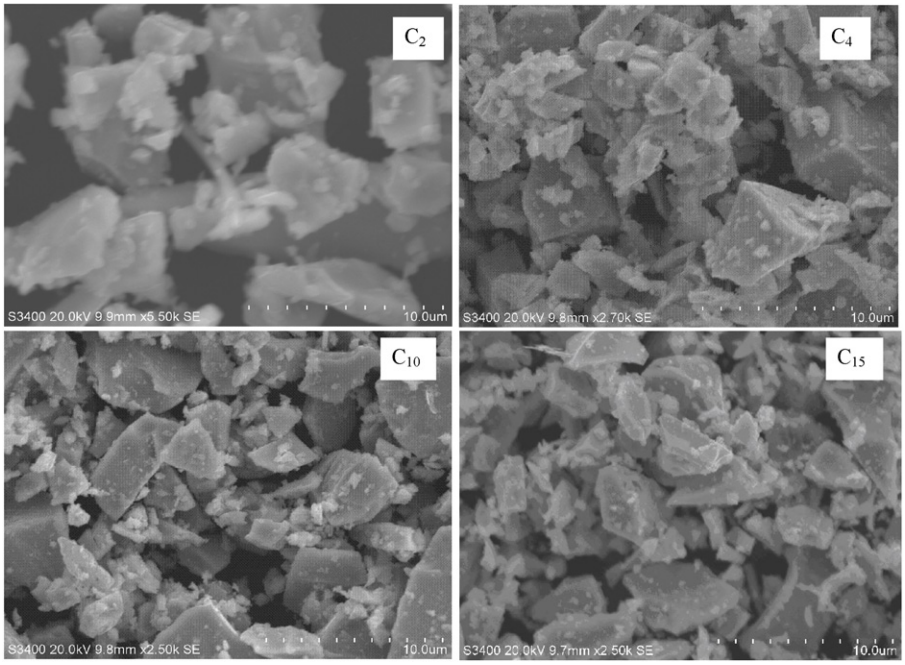

Figure 3. SEM pictures for some PbO–Sb_2O_3–B_2O_3:CoO glass ceramics.

Table 1. Physical parameters of PbO–Sb_2O_3–B_2O_3:CoO glass ceramics.

Glass ceramic	Avg. mol. wt.	Density (g cm^{-3})	Conc. of Co ions, N_i (10^{21} cm^{-3})	Inter-ionic distance of Co ions, r_i (Å)	Polaron radius, r_p (Å)
C_2	204.2	5.334	3.35	0.67	0.27
C_4	203.8	5.328	6.69	0.53	0.21
C_6	203.5	5.314	10.04	0.46	0.19
C_8	203.2	5.308	13.39	0.42	0.17
C_{10}	202.9	5.272	16.75	0.39	0.16
C_{15}	202.2	5.221	25.15	0.34	0.14
C_{20}	201.4	5.182	33.57	0.31	0.12

3. Results

The gradual increase of the content of the nucleating agent CoO in the glass matrix caused a slight decrease in the density of these ceramic materials (table 1).

From the measured values of the density and average molecular weight M of the samples, various other physical parameters such as cobalt ion concentration N_i, mean cobalt ion separation r_i and polaron radius r_p in PbO–Sb_2O_3–B_2O_3:CoO ceramic samples are computed and presented in table 1.

The prepared PbO–Sb_2O_3–B_2O_3:CoO glass ceramic samples contain well-defined, randomly distributed crystals ingrained in a glassy matrix. The residual glass phase is acting as interconnecting zones among the crystallized areas, making the samples free of voids and cracks. This is clear from the scanning microscopy pictures of the samples (figure 3). The pictures further indicate an increasing crystallinity with increasing concentration of CoO, the crystallizing agent. Thus, from these pictures it can also be concluded that CoO enhanced the phase separation tendency of various crystalline phases;

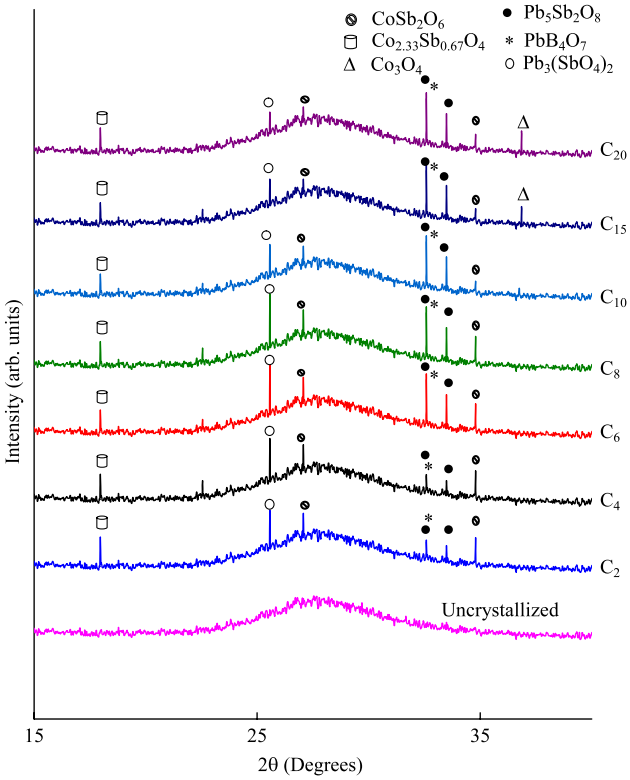

Figure 4. XRD patterns of PbO–Sb_2O_3–B_2O_3:CoO glass ceramics.

this fact reflects the specific overlap integral between the 3d levels of Co ion and the delocalized anti-bonding p-states of antimony. The chemical makeup of the crystal phases were characterized using EDS; the analysis indicated the presence of lead, boron, antimony, cobalt and oxygen elements in various crystalline phases. The distribution of the cobalt ions in

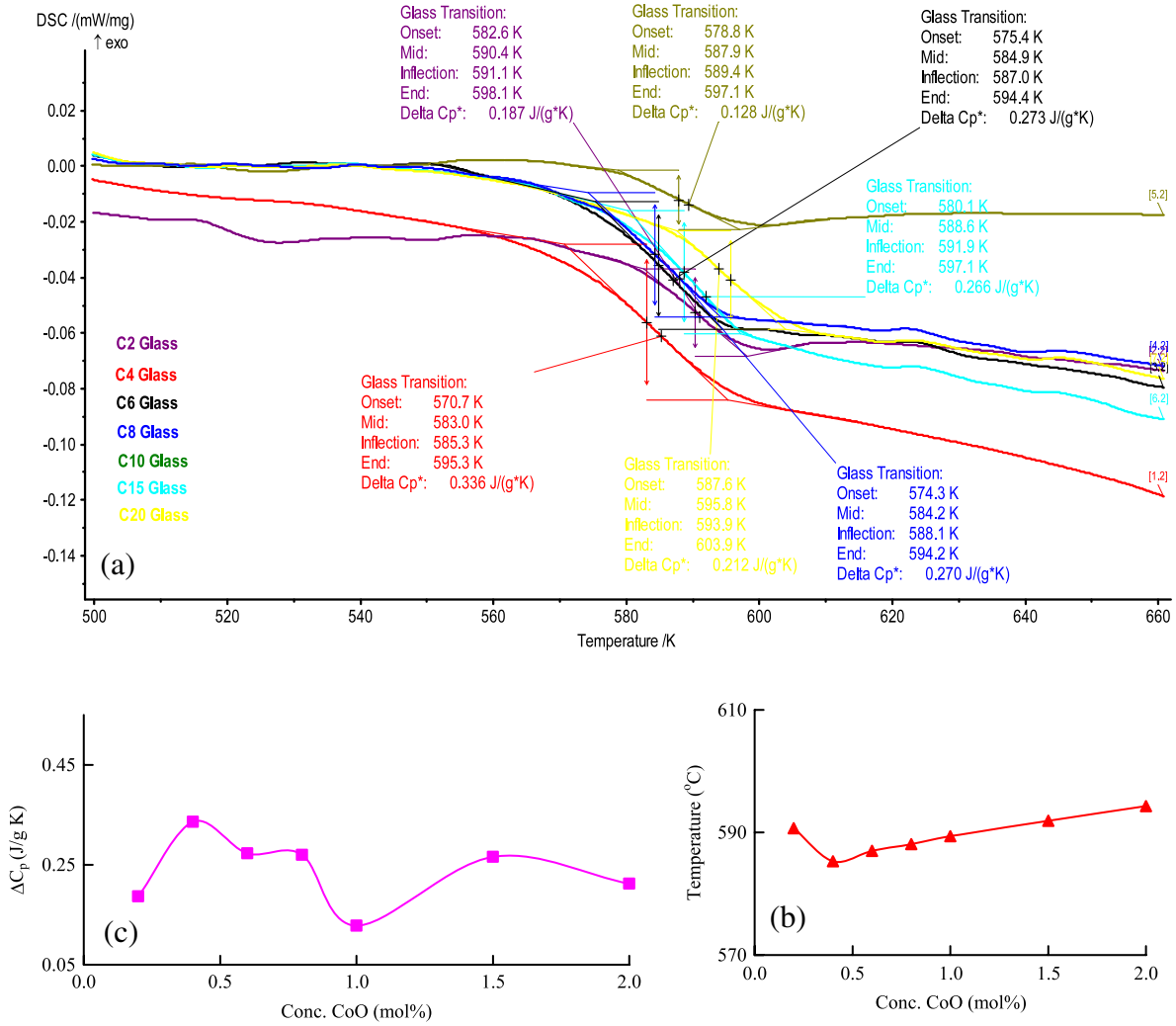

Figure 5. (a) DSC traces of PbO–Sb_2O_3–B_2O_3:CoO glass ceramics scanned in the low temperature region. (b) and (c) The variations of (b) glass transition temperature and (c) thermal capacity with the concentration of crystallizing agent CoO.

all the glass ceramic materials is also verified by recording x-ray maps for these samples. X-ray diffraction studies (figure 4) indicate the formation of $CoSb_2O_6$, $Co_{2.33}Sb_{0.67}O_4$, $Pb_5Sb_2O_8$, $Pb_3(SbO_4)_2$, PbB_4O_7 and Co_3O_4 crystalline phases in these samples (card nos, 18-0403, 15-0517, 22-0381, 01-0590, 15-0278 and 43-1003, respectively) [15]. The Co-rich areas in the samples may enhance the reactivity of the Co ion with the other oxides that precipitate as a high density of fine Co-rich crystals. These tiny crystals act as heterogeneous nuclei for the crystallization of the remaining glass. The diffraction data also indicate that, in these samples, the antimony ions exist in the Sb^{5+} state in addition to the Sb^{3+} state; however, the concentration of Sb^{3+} ions seems to be dominant over the Sb^{5+} ions in the samples crystallized with higher concentrations of CoO. The traces of Co^{3+} ions could also be seen in the samples C_{15} and C_{20}.

The average diameter of crystallites d_c is evaluated using Scherer's formula:

$$d_c = \frac{0.9\lambda}{\Delta\theta \cos\theta} \qquad (1)$$

where λ is the wavelength of x-rays and $\Delta\theta$ is the half-width of the diffraction peak; the maximum value of the diameter of the crystalline phases evaluated using this formula was found to be ∼60 nm. This order of diameter is sufficiently far away from the wavelengths of the visible and NIR spectral regions. In view of this, the scattering losses due to the difference of the refractive indices between crystallites and glass ceramics are expected to be negligibly small (less than 10^{-4}). Probably for this reason, these samples retain transparency even after crystallization.

In figure 5(a), we have shown differential scanning calorimetric (DSC) scans for PbO–Sb_2O_3–B_2O_3 glass ceramics with CoO contents ranging from 0.2 to 2.0 mol% in the temperature region 500–660 K. All DSC traces indicate typical glass transitions with the inflection point between 580 and 600 K. Although the inflection points of all the samples appear to be nearly the same, it is interesting that glass transition temperatures show an increasing trend with increase in the content of the nucleating agent (figure 5(b)), especially beyond 0.4 mol%. However, the variation of ΔC_p as a function of CoO content exhibits an oscillating behavior (figure 5(c)). In figure 6, the high temperature part of the DSC trace is

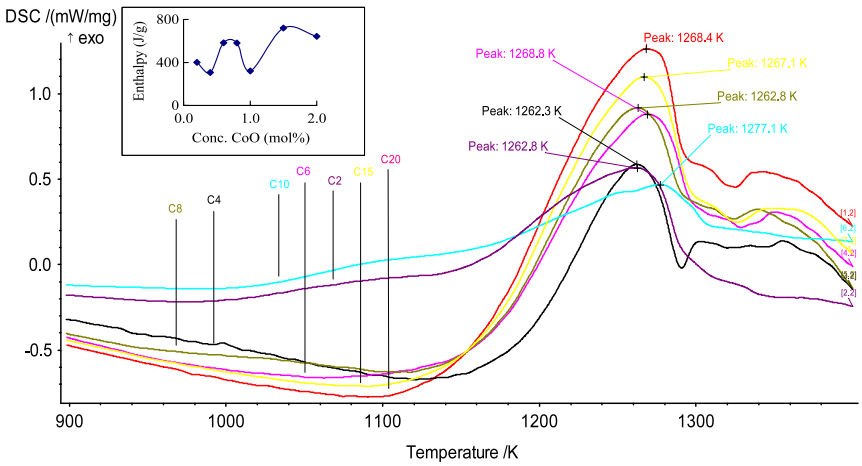

Figure 6. DSC traces of PbO–Sb_2O_3–B_2O_3:CoO glass ceramics scanned in the high temperature region. Inset shows the variation of enthalpy with the concentration of crystallizing agent CoO evaluated from the principal crystallization peak.

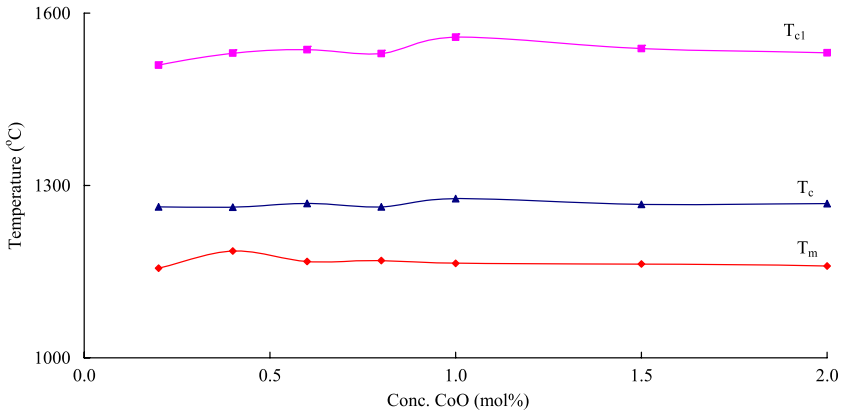

Figure 7. The variations of (a) crystallization temperature (onset), (b) crystallization peak temperature and (c) melting temperature with the concentration of crystallizing agent CoO.

presented. At about 1250 K, the DSC thermograms of each glassy alloys exhibit well-defined exothermic effects at the two steps of crystallization temperatures; the second peak appears to be very weak and spreads over a region of approximately 100 K (figure 6). An endothermic peak in the region of 1500–1560 K (not shown in the figure), due to the re-melting of the samples, is also observed in these traces. The variation of enthalpy associated with the primary crystallization peak with the concentration of crystallizing agent is shown as the inset in figure 6. The enthalpy is observed to increase (barring the sample C_{10}) with increase in the concentration of nucleating agent. A close look at the DSC trace of the sample C_{10} indicates that there are additional endothermic effects in the low temperature region which may account for the decrease of enthalpy associated with the primary peak. For the sample C_8, in figure 7, the variations of T_c (onset temperature of crystallization), T_{C1} (crystallization peak temperature) and T_m (melting temperature) with the concentration of nucleating agent are presented.

To observe the mass change effects during the heating process, we have also recorded thermal gravimetric traces for all the samples; in figure 8(a), TG traces for two of the samples are shown. These pictures predict that the decomposition process involves three successive steps. First, the decreasing mass of samples (mass reduction temperature onset), second, the increasing of mass up to the mass increase temperature peak and third, rapid mass lowering to the residual mass; the mass increasing peak corresponds well with the first crystallization peak. Figure 8(b) shows the dependence of onset mass reduction temperature and temperature of the mass increase peak as a function of CoO content. The summary of the data related to DSC studies is presented in table 2.

Figure 9 presents the optical absorption spectra for PbO–Sb_2O_3–B_2O_3:CoO glass ceramic samples recorded at room temperature in the spectral wavelength region 300–1800 nm. The absorption edge observed at 376 nm for the glass ceramic sample C_2 is found to be spectrally shifted gradually towards higher wavelength with increase in the concentration of nucleating agent CoO. Additionally, the spectrum of the sample C_2 exhibited a kink at about 528 nm (band 1) and two clearly resolved absorption bands at about 596 nm (band 2) and another band in the NIR region at about 1436 nm (band 3). As the concentration of crystallizing agent is increased, the half-width and the intensity of the last two bands are

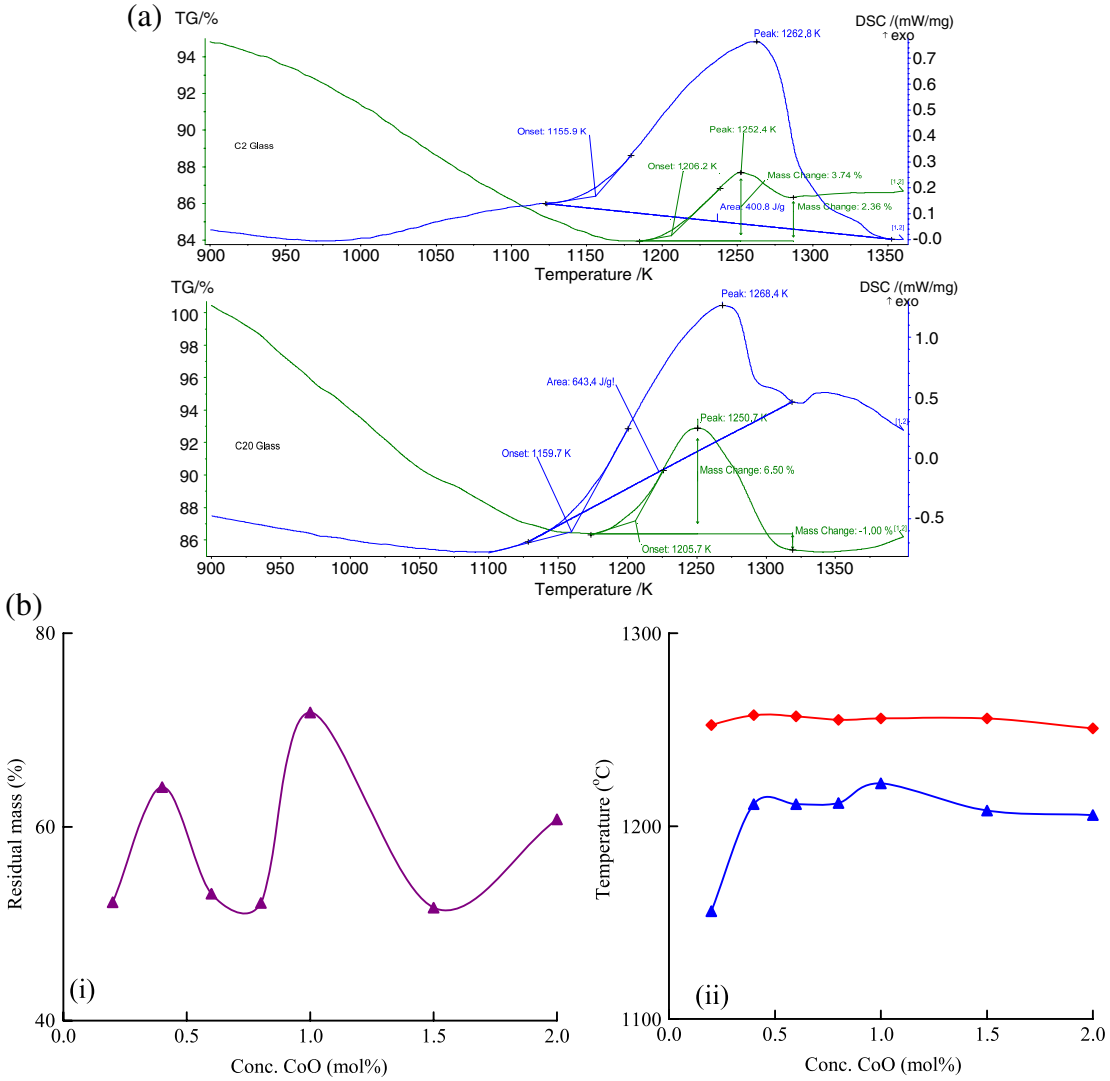

Figure 8. (a) Thermal gravimetry traces for the samples C_2 and C_{20}. (b) Variations of (i) residual mass, (ii) mass reduction temperature (onset) and mass increase temperature (peak) with the concentrations of crystallizing agent CoO.

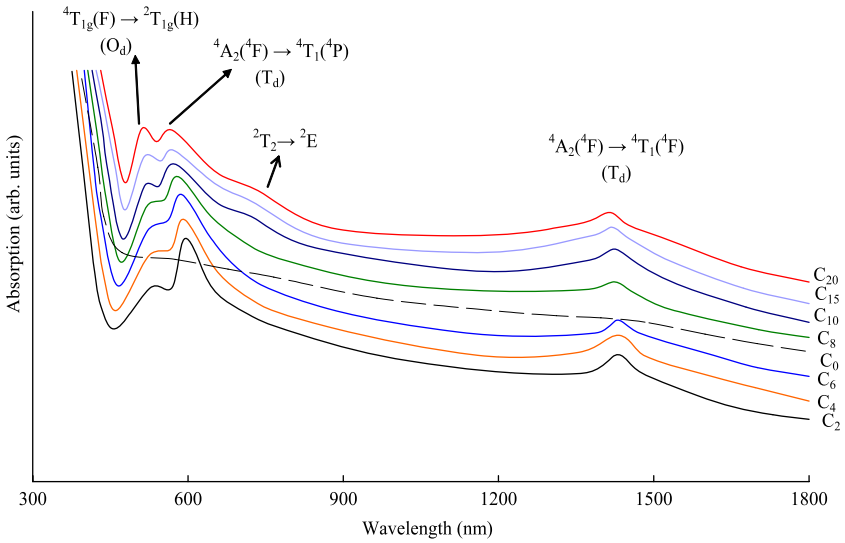

Figure 9. Optical absorption spectra of PbO–Sb_2O_3–B_2O_3:CoO glass ceramics recorded at room temperature.

Table 2. Summary of the data on differential scanning calorimetric studies of $PbO–Sb_2O_3–B_2O_3$:CoO glass ceramics.

Glass ceramic	CoO conc. (mol%)	Glass transition temp. (K) (inflection)	ΔC_p (J g^{-1} K^{-1})	Cryst. temp. onset (K)	Cryst. temp. (peak) (K) first step	Melting temp. onset (K)	Enthalpy of cryst. first step (J g^{-1})
C_2	0.2	591.1	0.187	1155.9	1262.8	1509.5	400.8
C_4	0.4	585.3	0.336	1185.8	1262.3	1530.4	306.8
C_6	0.6	587	0.273	1167.7	1268.8	1536.3	582.8
C_8	0.8	588.1	0.27	1169.3	1262.8	1529.6	581
C_{10}	1.0	589.4	0.128	1164.3	1277.1	1558.2	321.3
C_{15}	1.5	591.9	0.266	1163.3	1267.1	1538.4	720.4
C_{20}	2.0	593.9	0.212	1159.7	1268.4	1530.9	643.4

Table 3. Summary of the data on (a) the optical absorption spectra and (b) crystal field parameters of $PbO–Sb_2O_3–B_2O_3$:CoO glass ceramics.

(a)

			Position of band due to Co^{2+} ions (nm)		
Glass ceramic	Cutoff wavelength (nm)	Optical bandgap, E_o (eV)	$^4T_{1g}(F) \rightarrow {}^2T_{1g}(H)$ (O_d)	$^4A_2(4F) \rightarrow {}^4T_1(4P)$ (T_d)	$^4A_2(4F) \rightarrow {}^4T_1(4F)$ (T_d)
C_2	376	2.68	528	596	1436
C_4	385	2.60	524	593	1433
C_6	399	2.52	522	588	1430
C_8	406	2.36	520	581	1424
C_{10}	415	2.32	517	574	1423
C_{15}	423	2.24	515	572	1418
C_{20}	432	2.16	510	570	1414

(b)

	Crystal field parameters (cm^{-1})			
Glass ceramic	Dq	B	C	Nephelauxetic ratio (β)
C_2	−402	779	3505	0.802
C_4	−403	784	3528	0.807
C_6	−403	793	3568	0.817
C_8	−405	806	3627	0.830
C_{10}	−405	820	3690	0.844
C_{15}	−406	823	3703	0.848
C_{20}	−407	826	3717	0.851

observed to decrease whereas band 1 is observed to grow at the expense of these two bands. Furthermore, a weak kink at about 714 nm in the spectra of C_{15} and C_{20} could also be visualized. From the observed absorption edges, we have evaluated the optical bandgaps (E_o) of these samples by drawing Urbach plots between $(\alpha\hbar\omega)^{1/2}$ and $\hbar\omega$. The values of the optical bandgap (E_o) are determined and are presented in table 3(a) along with the other relevant data. The value of E_o is observed to decrease with increase in the concentration of CoO.

The data on magnetic susceptibility (χ) of $PbO–Sb_2O_3–B_2O_3$:CoO glass ceramics measured at room temperature are presented in table 4; the value of χ is observed to increase gradually with increase in the content of CoO. From the values of magnetic susceptibilities, the magnetic moment (μ) of the Co^{2+} ion is evaluated by taking the concentration of Co^{2+} ions from table 1 and presented in table 4. For the samples C_2 to C_{10}, μ is found to be in the range of 3.9–4.5 μ_B whereas for the samples C_{15} and C_{20}, it is found to be ∼5.0 μ_B.

Figure 10 represents the comparison plot of the change of photo-induced birefringence with the photo-inducing power; we observe a substantial increase of the PIB output with the increase of the pumping power for all the samples. In the inset

Table 4. Summary of the data on magnetic susceptibility of $PbO–Sb_2O_3–B_2O_3$:CoO glass ceramics.

Glass ceramic	χ ($\times 10^{-6}$ emu)	μ (μ_B)
C_2	35.2	3.92
C_4	79.4	4.16
C_6	126.1	4.28
C_8	171.4	4.32
C_{10}	227.4	4.45
C_{15}	414.0	4.95
C_{20}	622.3	5.20

of figure 10, we have presented photo-induced birefringence with the concentration of the crystallizing agent measured with the pump power density, 0.8 GW cm^{-2} ($\lambda = 1064$ nm); the figure indicates a slow increase of PIB intensity up to 0.6 mol% concentration of nucleating agent, and for further increases of CoO content a rapid increase could be observed.

Figure 11 shows luminescence emission spectra recorded at room temperature of $PbO–Sb_2O_3–B_2O_3$:CoO glass ceramic samples excited at the wavelength corresponding to band 2 in the absorption spectra. The spectra of all the samples

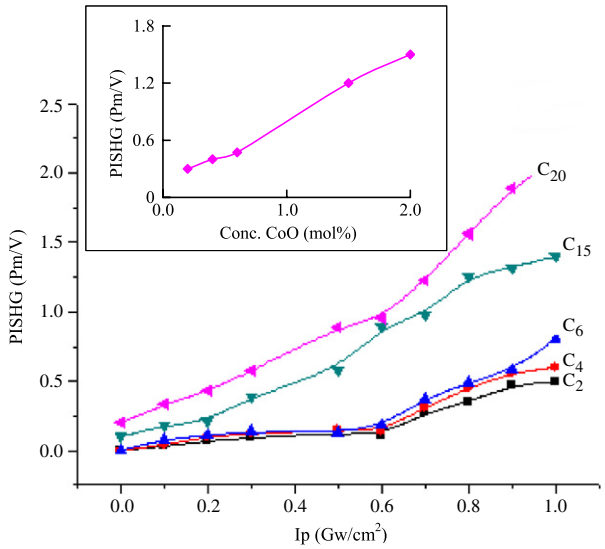

Figure 10. Comparison plot of the change of photo-induced birefringence with the photo-inducing power. Inset shows the variation of photo-induced birefringence with the concentration of the crystallizing agent measured with the pump power density, 0.8 GW cm^{-2} ($\lambda = 1064$ nm).

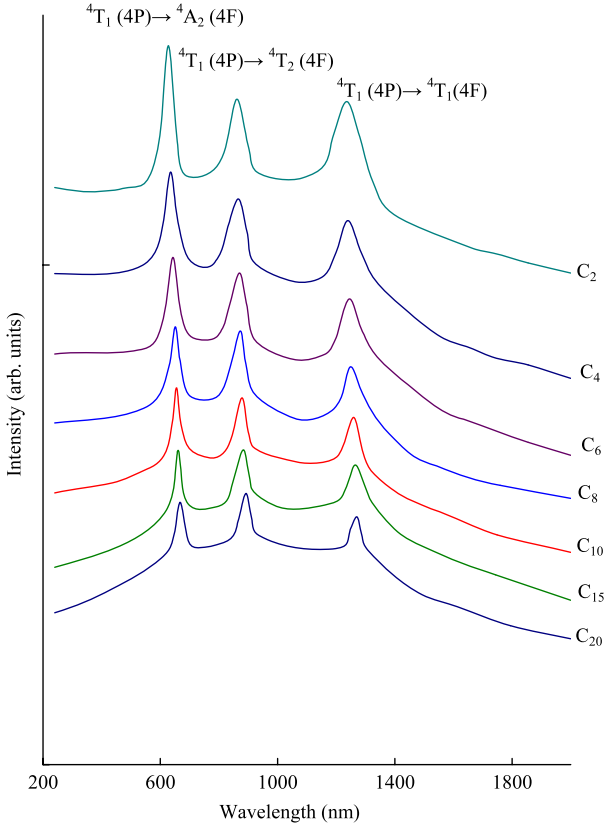

Figure 11. Emission spectra for some of the PbO–Sb_2O_3–B_2O_3:CoO glass ceramics.

exhibited three emission bands with peak positions varying in the regions 620–675 nm, 860–890 nm and 1235–1270 nm; as the concentration of the nucleating agent is increased, a gradual diminishing of these bands is observed.

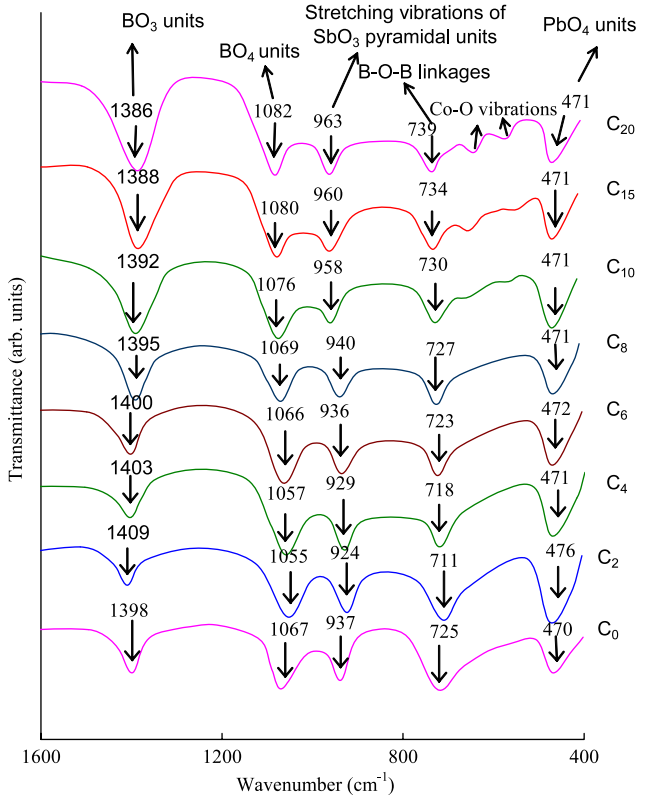

Figure 12. IR spectra of PbO–Sb_2O_3–B_2O_3:CoO glass ceramics.

The infrared transmission spectrum of glass ceramic sample C_2 (figure 12) exhibited three conventional bands originating from borate groups at 1409 cm^{-1} (due to BO_3 units), 1055 cm^{-1} (due to BO_4 units) and another band at 711 cm^{-1} due to bending vibrations of B–O–B linkages [16]. In the spectrum of this sample, the ν_1 vibrational band of SbO_3 units appeared at 925 cm^{-1} whereas the ν_2 and ν_4 bands seem to be missing. The ν_3 vibrational bands merged with the band due to bending vibrations of B–O–B linkages and may have formed a common vibrational band due to B–O–Sb linkages. In addition, a band due to PbO_4 structural groups at about 472 cm^{-1} [17] is also observed in the spectra of all the samples. With the gradual increase in the concentration of crystallizing agent CoO, the intensity of BO_3 and SbO_3 structural units is observed to increase (with a shift towards lower wavenumber) whereas that of the bands due to BO_4 structural units is observed to decrease. Interestingly, two new intense kinks (especially in the spectra of the samples C_{15} and C_{20}) at about 640 and 570 cm^{-1} could also be observed; these kinks are identified due to vibrations of Co^{III}–O bonds [18]. The summary of the data on IR spectra is presented in table 5.

Figure 13 shows the Raman spectra of PbO–Sb_2O_3–B_2O_3:CoO glass ceramics. The spectra show some noise due to specific stability of the laser sources and probably due to some inclusions in the glasses. However, this noise does not influence the spectral positions of the phonon modes. Such a situation occurs very often for the glass, polymer, disordered and amorphous materials.

The spectrum of the sample C_2 exhibited a weak band at about 1040 cm^{-1}, identified due to diborate groups consisting

Table 5. Summary of the data on various band positions (cm^{-1}) in IR spectra of $PbO–Sb_2O_3–B_2O_3$:CoO glass ceramics.

Glass ceramic	Borate groups (cm^{-1})			SbO_3 groups ν_1 (cm^{-1})	Band due to PbO_4 units (cm^{-1})	Co–O groups (cm^{-1})
	BO_3	BO_4	B–O–B			
C_0	1398	1067	725	937	470	—
C_2	1409	1055	711	924	476	—
C_4	1403	1057	718	929	471	—
C_6	1400	1066	723	936	472	—
C_8	1395	1069	727	940	471	—
C_{10}	1392	1076	730	958	471	655, 565
C_{15}	1388	1080	734	960	471	654, 548
C_{20}	1386	1082	739	963	471	642, 572

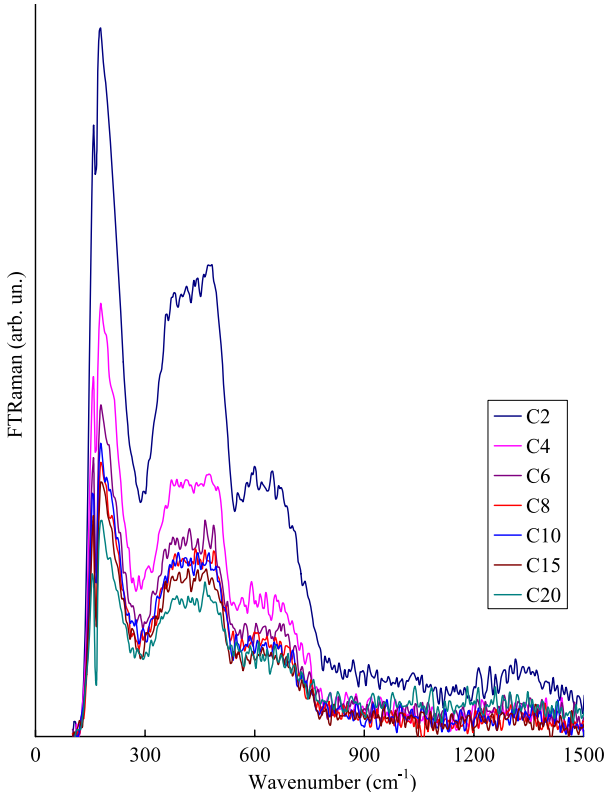

Figure 13. FT Raman spectra of $PbO–Sb_2O_3–B_2O_3$:CoO glass ceramics.

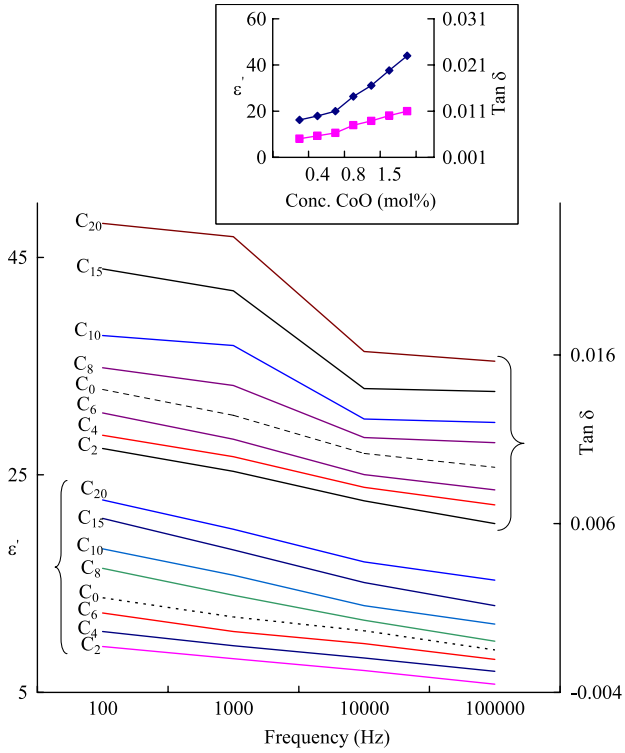

Figure 14. The variation of dielectric constant and loss of $PbO–Sb_2O_3–B_2O_3$:CoO glass ceramics with frequency at room temperature. Inset shows the variation of dielectric constant and loss at 1 kHz with the concentration of CoO.

of six-membered rings containing two BO_4 tetrahedra and another band centered at 820 cm^{-1}, ascribed to the boroxyl ring oxygen breathing in which the boron coordinate atom is three [19]; a band due to chain-type meta-borate groups is also detected at about 690 cm^{-1}. Additionally, the spectrum consists of a broad band over the region of 350–500 cm^{-1}; this region consists of bands due to symmetric stretching vibrations of SbO_3 pyramids and a band due to isolated BO_4 structural units [20]. A wide band spreading over the region of 1300–1400 cm^{-1} is also observed in the spectrum of this sample; we attribute this band to an overlap of the following modes: (1) $B\text{Ø}_2O^-$ triangle linked to $B\text{Ø}_4$ unit (here Ø is the oxygen atom bridging to two boron atoms); (2) $B–O^-$ in $B\text{Ø}_2O^-$ triangle [21, 22] and (3) stretching in $B\text{Ø}_3$ triangles. The spectrum also exhibits an intense band at about 175 cm^{-1}; this band represents the vibrations of fourfold-coordinated Pb^{2+} at the apex of the PbO_4 pyramid [23]. As the concentration of the crystallizing agent is increased, there is a diminishing intensity of bands due to BO_4 structural units. Further, the common band observed in the region of 350–500 cm^{-1} is gradually resolved into two separate bands; a band due to symmetric stretching vibrations of Sb–O–Sb bridges and a weak band due to BO_4 structural units.

The dielectric constant ε' and loss $\tan\delta$ at room temperature (≈30 °C) of pure $PbO–Sb_2O_3–B_2O_3$ pre-crystallized glasses at 100 kHz are measured to be 8.9 and 0.0093, respectively. Figure 14 represents the variation of dielectric constant and loss with frequency at room temperature of $PbO–Sb_2O_3–B_2O_3$ glasses crystallized with different concentrations of CoO; the inset of the same figure shows the variation of these parameters with the concentration of crystallizing

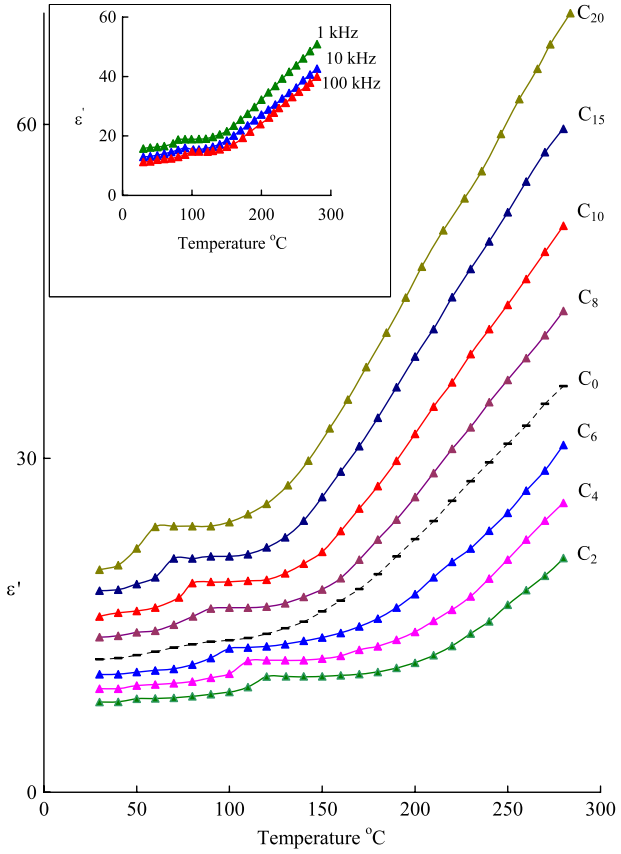

Figure 15. Comparison plot of variation of dielectric constant at 1 kHz with temperature for PbO–Sb_2O_3–B_2O_3:CoO glass ceramics. Inset shows the variation of dielectric constant for glass ceramic C_{10} at different frequencies.

agent CoO measured at 1 kHz. The parameters, ε' and $\tan\delta$ are observed to increase with the concentration of CoO. The temperature dependence of ε' at 1 kHz of PbO–Sb_2O_3–B_2O_3 glasses crystallized with different concentrations of CoO is shown in figure 15 and at different frequencies of the glass ceramic sample C_{10} is shown as the inset. The value of ε' is found to exhibit a considerable increase at higher temperatures, especially at lower frequencies; the rate of increase of ε' with temperature is found to increase with increase in the concentration of crystallizing agent.

A comparison plot of variation of $\tan\delta$ with temperature, measured at a frequency of 10 kHz for all the glass ceramic samples is presented in figure 16(a). The inset of this figure represents the temperature dependence of $\tan\delta$ of sample C_6 at different frequencies. Variation of dielectric loss with frequencies for the sample C_{20} measured at different temperatures is shown in figure 16(b). These curves have exhibited distinct maxima; with the increase in frequency the temperature maximum of $\tan\delta$ shifts towards higher temperatures and with the increase in temperature, the frequency maximum shifts towards higher frequencies, indicating the relaxation character of dielectric losses in these glass ceramics. From these curves, it is also observed that the region of relaxation shifts towards lower temperatures with broadening of the relaxation peaks and an increasing value

Table 6. Dielectric properties of PbO–Sb_2O_3–B_2O_3:CoO glass ceramics.

Glass ceramic	$(\text{Tan}\,\delta)_{\text{Max.Avg}}$	Temp. region of relaxation (°C)	AE for dipoles (eV)	AE for conduction (eV)
C_2	0.0101	110–150	3.0	0.68
C_4	0.0115	101–143	2.95	0.57
C_6	0.0131	90–133	2.79	0.51
C_8	0.0175	84–130	2.65	0.43
C_{10}	0.0201	80–128	2.51	0.39
C_{15}	0.0226	70–121	2.37	0.33
C_{20}	0.0253	65–119	2.24	0.29

of $(\tan\delta)_{\max}$ with the increase in the concentration of the nucleating agent. The effective activation energy W_d for the dipoles is evaluated for all the glass ceramic samples using the relation

$$f = f_o e^{-W_d/kT} \tag{2}$$

and is presented in table 6; the activation energy is found to decrease gradually with increase in the concentration of the crystallizing agent. The other pertinent data related to dielectric loss of these glass ceramics is presented in table 6.

The ac conductivity σ_{ac} is calculated at different temperatures, using the relation

$$\sigma_{ac} = \omega\varepsilon_o\varepsilon'\tan\delta \tag{3}$$

for different frequencies and the plots of $\log\sigma_{ac}$ against $1/T$ are shown in figure 17 for all the glass ceramics at 100 kHz. From these plots, the activation energy for conduction in the high temperature region over which a near-linear dependence of $\log\sigma_{ac}$ with $1/T$ could be observed is evaluated and presented in table 6; this activation energy is also found to decrease gradually with increase in the concentration of the crystallizing agent.

4. Discussion

The PbO–Sb_2O_3–B_2O_3:CoO glass ceramic is an admixture of network former, intermediate and modifiers. In this system, Sb_2O_3 is an incipient glass network former and, as such, does not readily form a glass but does so in the presence of modifier oxides like PbO and the glass former B_2O_3. Antimony oxide participates in the glass network with SbO_3 structural units with the oxygen at three corners and the lone pair of electrons of antimony at the fourth corner as mentioned earlier. In the glass network, normally the Sb–O distances lie in between 2.0 and 2.6 Å [24–26]. The coordination polyhedra are joined by sharing the corners to form double infinite chains with the lone pairs pointing out from the chains. These chains are held together by weak secondary Sb–O bonds with lengths greater than 2.6 Å. X-ray diffraction studies of the present investigation have indicated that antimony ions also exist in the Sb^{5+} state in these glass ceramics. Earlier EXAFS studies on antimony borate glasses have indicated that SbO_3 trigonal pyramids are less compatible with the BO_4 units in the glass network. The reasons are obvious; the Sb^{3+} ion with its lone electron pair occupies a greater angular volume than a bonding

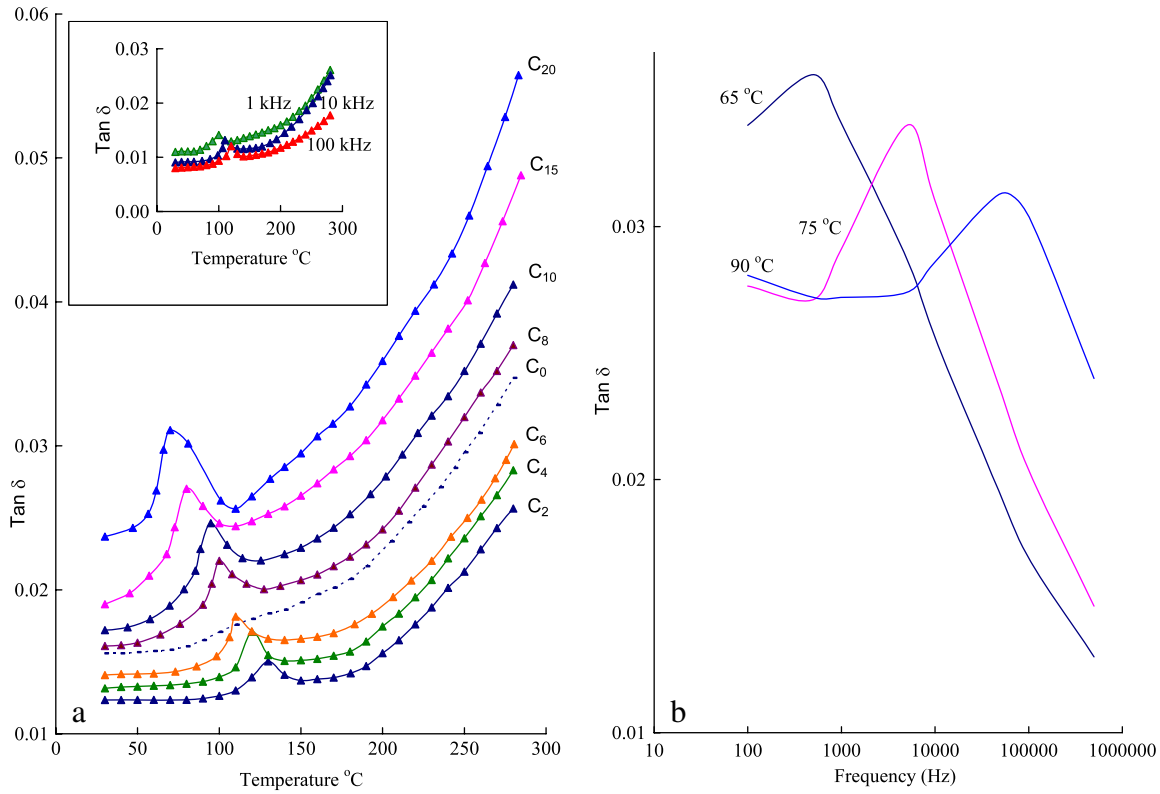

Figure 16. (a) Comparison plot of variation of dielectric loss at 10 kHz with temperature for PbO–Sb_2O_3–B_2O_3:CoO glass ceramics. Inset shows the variation of dielectric loss with temperature for glass ceramic C_6 at different frequencies. (b) Variation of dielectric loss with frequencies for the glass C_{20} measured at different temperatures.

pair of electrons. As a participant of the glass network, the local structure of Sb^{3+} cations becomes less symmetric and the strain energy in the glass network increases as a whole, thus resulting in a decrease in the additional activation energy that is necessary for glass network rearrangement. As a result we expect more degrees of disorder in glass ceramics containing Sb^{3+} ions rather than in the glass ceramics containing Sb^{5+} ions. Sb^{5+} ions participate in the glass network with $Sb^{V}O_4$ units and play a similar structural role with BO_4 units and may form cross linkages of the type Sb–O–B with the BO_4 units [27]. B_2O_3 is a well-known network former with BO_3 and BO_4 structural units. PbO in general is a glass modifier and enters the glass network by breaking up the Sb–O–Sb, Sb–O–B and B–O–B bonds (normally the oxygens of PbO break the local symmetry while Pb^{2+} ions occupy interstitial positions) and introduces coordinate defects known as dangling bonds along with non-bridging oxygen ions. In this case the lead ions are octahedrally positioned; to form octahedral units, Pb should be sp^3d^2-hybridized (6s, 6p and 6d orbitals) [28, 29]. However, PbO may also participate in the glass network with [$PbO_{4/2}$] pyramidal units connected in puckered layers. Cobalt ions are expected to exist mainly in the Co^{2+} state in the PbO–Sb_2O_3–B_2O_3:CoO glass network. However, the oxidation of cobalt ions from Co^{2+} to Co^{3+} appears to be possible during melting, annealing and crystallization processes of the glasses. Co^{2+} ions occupy both octahedral and tetrahedral positions whereas Co^{3+} ions occupy mainly octahedral positions in the glass network [30].

In general, the degree of structural compactness, the modification of the geometrical configuration of the glassy network, the size of the micro-crystals formed, the change in the coordination of the glass forming ions and the fluctuations in the dimensions of the interstitial holes are some of the factors that influence the density of the glass ceramic material. In the present case, progressive introduction of crystallizing agent CoO caused a slight decrease in the density; this is indicative of the decreasing structural compactness of the material. It is also evocative of the decreasing presence of Sb^{5+} ions whose field strength is higher (when compared with that of the Sb^{3+} state) that makes the sample less compact.

The formation of $CoSb_2O_6$, $Co_{2.33}Sb_{0.67}O_4$ and $Pb_3(SbO_4)_2$ crystalline phases detected from the XRD studies indicate the presence of Sb^{5+} ions in these glass ceramics. The relative variation in the intensity of the diffraction patterns also indicates a decreasing concentration of these ions with the increase in the concentration of nucleating agent. XRD studies also indicate the formation of Co_3O_4 crystallization phases, especially in the samples C_{15} and C_{20}; the presence of these phases confirms the conversion of a fraction of cobalt ions into the Co^{3+} state in these glass ceramics.

The analysis of the results of DSC studies indicates that, with the increase in the concentration of crystallizing agent CoO, there is a considerable increase in the glass transition temperature T_g. As per the empirical relation of Tanaka [31], the relation between T_g and the average coordination number

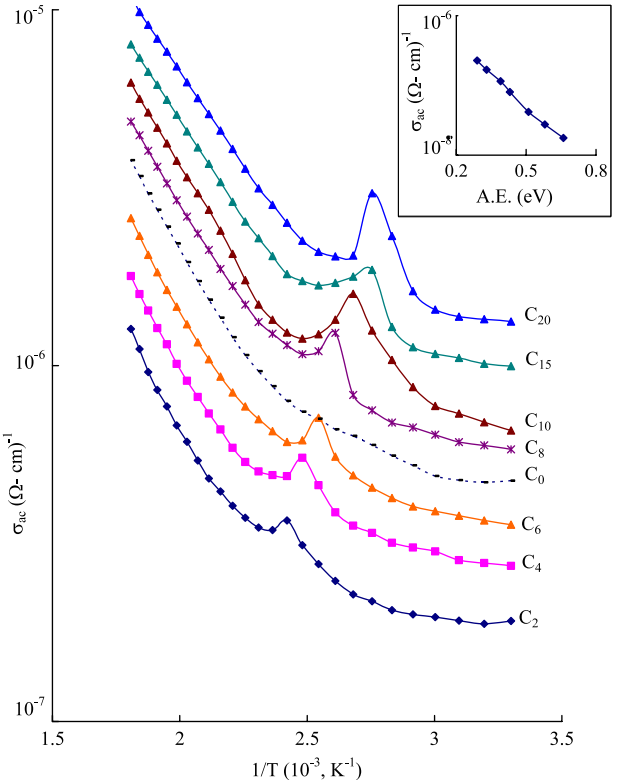

Figure 17. A comparison plot of ac conductivity with $1/T$ at 100 kHz for PbO–Sb_2O_3–B_2O_3:CoO glass ceramics. Inset shows the variation of activation energy for conduction with the concentration of CoO.

(Z) is represented by

$$\ln T_g \approx 1.6Z + 2.3. \quad (4)$$

This equation clearly suggests that the higher the value of T_g, the higher is the average coordination number; our observations on the glass transition temperature for the present samples are well in accordance with this equation. The appearance of different crystallization temperatures in the DSC pattern obviously suggests the presence of different phases of crystallization in the samples. The crystallization in the glass samples may take place following the surface and bulk nucleations. The general shape of the crystallization peak in DSC curves reflects the variation of enthalpy. The increase in the value of enthalpy with the increase in the nucleating agent suggests that the crystallization starts initially inside the material and expands to the surface gradually [32]. TG measurements suggest the temperature at which maximum mass reduction takes place shifts towards lower temperature with increase in the concentration of nucleating agent. This result also suggests a growing degree of disorder with increase in the concentration of CoO.

The electronic spectra of the Co^{2+} ions in glass and glass ceramics are well known [33]. The crystal field splitting of the energy levels of Co^{2+} (d^7) ions in a tetrahedral field is just similar to the d^3 electronic configuration in an octahedral field [3, 34]. The tetrahedral field splits the ground state ^4F into $^4A_2$, $^4T_2$ and $^4T_1$ levels, with $^4A_2$ as the lowest. Using Tanabe–Sugano diagrams for the d^3 configuration, which is conjugate to the (d^7) ion, the absorption peak observed near 600 nm is assigned to $^4A_2(^4F) \rightarrow {}^4T_1(^4P)$ and the band observed in the NIR region (at about 1400 nm) is assigned to $^4A_2(^4F) \rightarrow {}^4T_1(^4F)$. The crystal field parameters (Dq, B and C) evaluated for these spectra are furnished in table 3(b). The pattern of the absorption spectra and the negative values of the Dq obtained clearly suggest that Co^{2+} ions are largely located in tetrahedral sites, especially in the initial set of the samples investigated. The nephelauxetic ratio (β) evaluated from the Racah parameter (B) shows an increasing trend; such a trend clearly suggests the decrease of the covalency around Co^{2+} as the concentration of the nucleating agent is increased. In the spectra, we have also observed the shifting of the octahedral bands towards lower wavelengths as the concentration of CoO is increased; such a shift in the position of the bands indicates the decrease in average distance of Co–O. Yet, the spectra exhibited a new band that is growing at the expense of the tetrahedral bands, at about 520 nm; this band is identified due to $^4T_{1g}(F) \rightarrow {}^2T_{1g}(H)$ octahedral transition of Co^{2+} ions [35]. Further, a kink at about 720 nm could also be detected in the spectra of samples C_{10}–C_{20}. This band is identified due to the $^5T_2 \rightarrow {}^2E$ transition of octahedrally positioned Co^{3+} ions [36]. Thus the optical absorption spectra also indicate that part of the cobalt ions exists in the Co^{3+} state, especially in the samples crystallized with higher concentrations of CoO. The increasing intensity and the width of the $^4T_{1g}(F) \rightarrow {}^2T_{1g}(H)$ octahedral band suggests a gradual transformation of Co^{2+} ions from tetrahedral to octahedral positions. We have also observed a decrease in the optical bandgap with increase in the concentration of crystallizing agent. The octahedrally coordinated Co^{2+} ions act as a modifier similar to Pb^{2+} ions and induce non-bridging oxygens (NBOs) in the glass ceramic network. The higher the concentration of these modifier ions, the higher is the concentration of NBOs in the glass matrix. This leads to an increase in the degree of localization of electrons, thereby increasing the donor centers in the glass ceramic matrix. The presence of larger concentrations of these donor centers decreases the optical bandgap and shifts the absorption edge towards the higher wavelength side as observed. More specifically, the redshift of E_g with the increase in the content of CoO is associated with a decrease in the exchange interactions between the p electrons in the conduction band in Sb_2O_3 and the localized d electrons of the substitutionally (tetrahedrally) positioned cobalt ions.

The experiments on PIB indicated the maximum intensity of birefringence for the sample C_{20}; it is very crucial because the same sample is possessing a minimal optical energy gap and crystal field strength. This is a very important result in the current investigation because it allows us to conclude that Co ions surrounding ligands play a principal role in the observed PIB. To be more specific, the octahedrally coordinated Co^{2+} ions contribute more significantly to NLO effects. The higher concentration of Sb^{3+} ions (when compared with the Sb^{5+} ions) is also another factor for the larger intensity of PIB for this sample (C_{20}).

The luminescent transitions for tetrahedral Co^{2+} ions can be determined by the relative locations of $^4T_1(^4P)$ and $^2E(^2G)_1$ excited states. Out of these, the emissions from the

^{2}E metastable state are expected to be a very narrow set of emission bands, as was reported in a number of crystalline and glass ceramic materials [33, 37]. Hence it is justified that, in the present case, we assign the red emission band observed at about 660 nm to $^4T_1(^4P) \rightarrow {}^4A_2(^4F)$ whereas NIR bands observed at about 870 nm and at about 1270 nm are assigned to the $^4T_1(^4P) \rightarrow {}^4T_2(^4F)$ and $^4T_1(^4P) \rightarrow {}^4T_1(^4F)$ transitions of tetrahedrally positioned Co^{2+} ions, respectively. The quenching of luminescence emission with increase in the content of CoO is either due to the decreasing concentration of tetrahedral Co^{2+} ions in the glass ceramic and/or may be due to non-radiative relaxation processes.

The magnetic susceptibility for PbO–Sb_2O_3–B_2O_3:CoO glass ceramics arises prevailingly due to paramagnetic $Co^{2+}(3d^7)$ ions. Normally, for the octahedrally coordinated Co^{2+} ions the value of μ_{eff} lies in the range 4.7–5.2 μ_B whereas for the tetrahedrally coordinated Co^{2+} ions, the range of μ_{eff} is 3.8–4.5 μ_B [38, 39]. From the data on magnetic susceptibility measurements and the range of magnetic moments obtained for the present glass ceramics, it can be concluded that in the samples C_2 to C_{10}, Co^{2+} ions exist mostly in tetrahedral positions whereas in the samples C_{15} and C_{20}, Co^{2+} ions occupy predominantly octahedral positions.

In the IR spectra, with the gradual increase in the concentration of crystallizing agent CoO, the intensity of BO_3 and SbO_3 structural units is observed to increase whereas that of the bands due to BO_4 structural units is observed to decrease. Tetragonally positioned Co^{2+} ions do not induce any dangling bonds but octahedrally positioned Co^{2+} ions may do so [40] similar to Pb^{2+} ions. The gradual increase in the intensity of the bands due to BO_3 and SbO_3 structural units indicates the increasing presence of cobalt ions in octahedral positions. The additional feature of the IR spectra is that there are two absorption bands at about 640 and 570 cm^{-1} in the spectra of the samples C_{15} and C_{20}. These bands are attributable to the vibrations of Co^{III}–O bonds in Co_3O_4 crystalline phases [1, 16]. Thus this result clearly suggests that, in the samples crystallized with higher concentrations of CoO, cobalt ions not only exist in the Co^{3+} state in addition to Co^{2+} but also form a Co_3O_4 crystalline phase (as observed in the XRD study) which plays a crucial role in NLO effects and electrical properties of these samples.

The revelations of Raman spectral studies on these samples are also more or less the same. The decrease in the intensity of the band due to BO_4 structural units and the splitting of the common vibration band observed in the region 350–500 cm^{-1} into two separate bands with the increase in the concentration of crystallizing agent supports the viewpoint that there is an increasing concentration of octahedrally positioned cobalt ions that act as modifiers in the glass ceramic network.

The values of dielectric parameters, namely ε', $\tan\delta$ and σ_{ac}, at any frequency are found to increase with temperature and the activation energy for ac conduction is observed to decrease with increase in the content of nucleating agent CoO; this is an indication of an increase in the space charge polarization. Such an increase is probably due to the increasing concentration of Co^{2+} ions that act as modifiers in these samples. These modifying ions, as mentioned earlier, generate bonding defects in the glass network. The defects thus produced create easy pathways for the migration of charges that would build up space charge polarization and facilitate an increase in the dielectric parameters, as observed [41–43].

The value of the effective activation energy associated with the dipoles is observed to decrease with increase in the content of cobalt ions in the glass ceramic network (table 6). This observation points out an increasing freedom for dipoles to orient in the field direction, obviously due to the increasing degree of disorder in the glass ceramic network. The observed dielectric relaxation effects in PbO–Sb_2O_3–B_2O_3 glasses crystallized with different concentrations of CoO may be attributed to the association of octahedrally positioned Co^{2+} ions with a pair of cationic vacancies as observed in a number of conventional glasses, glass ceramics and crystals that contain divalent positive ions, as reported before [44].

Although the conventional Cole–Cole plot method is very useful for describing relaxation effects, it is preferable sometimes to determine the relaxation parameters by a graphical method suggested by Cole [45]. Combination of the standard Debye relations:

$$\varepsilon'(\omega) = \varepsilon_\infty + \frac{\varepsilon_s - \varepsilon_\infty}{1 + \omega^2\tau^2} \tag{5}$$

$$\varepsilon''(\omega) = \frac{(\varepsilon_s - \varepsilon_\infty)\,\omega\tau}{1 + \omega^2\tau^2}, \tag{6}$$

gives rise to

$$\varepsilon''(\omega)\omega = \frac{(\varepsilon_s - \varepsilon_\infty)\,\omega\tau}{1 + \omega^2\tau^2} = \frac{1}{\tau}\left(\varepsilon_s - \varepsilon'(\omega)\right), \tag{7}$$

$$\varepsilon''(\omega)/\omega = \frac{(\varepsilon_s - \varepsilon_\infty)\,\tau}{1 + \omega^2\tau^2} = \tau\left(\varepsilon'(\omega) - \varepsilon_\infty\right). \tag{8}$$

The equations (7) and (8) yield straight lines with slopes $1/\tau$ and τ, respectively. In the present measurements for one of the glass ceramic samples, namely, sample C_{20}, the plots between $\varepsilon''(\omega)\omega$ versus $\varepsilon'(\omega)$ and $\varepsilon''(\omega)/\omega$ versus $\varepsilon'(\omega)$ are shown in figure 18. The plots are observed to be straight lines indicating the dipolar relaxation effects in these samples; a slight deviation from the straight line is observed in the high frequency region for these graphs. Such a deviation suggests spreading of relaxation times. Graphs drawn for other glass ceramics have also exhibited nearly the same behavior. The spreading of relaxation times in these glass ceramics may be understood due to the experience of an approximately random potential energy on diffusing through the distorted structure of a PbO–Sb_2O_3–B_2O_3:CoO glass ceramic network by the dipoles [46].

The variation of $\log\sigma(\omega)$ versus activation energy for conduction (in the high temperature region) is shown as an inset in figure 17; the graph yields a near-straight line. This observation suggests that the conductivity enhancement is directly related to the thermally stimulated mobility of the charge carriers in the high temperature region. The progressive increase of conductivity with the increase of cobalt content in the glass ceramic is a manifestation of the increasing concentration of mobile electrons, or polarons, involved in the process of transfer from Co^{2+} to Co^{3+}. The

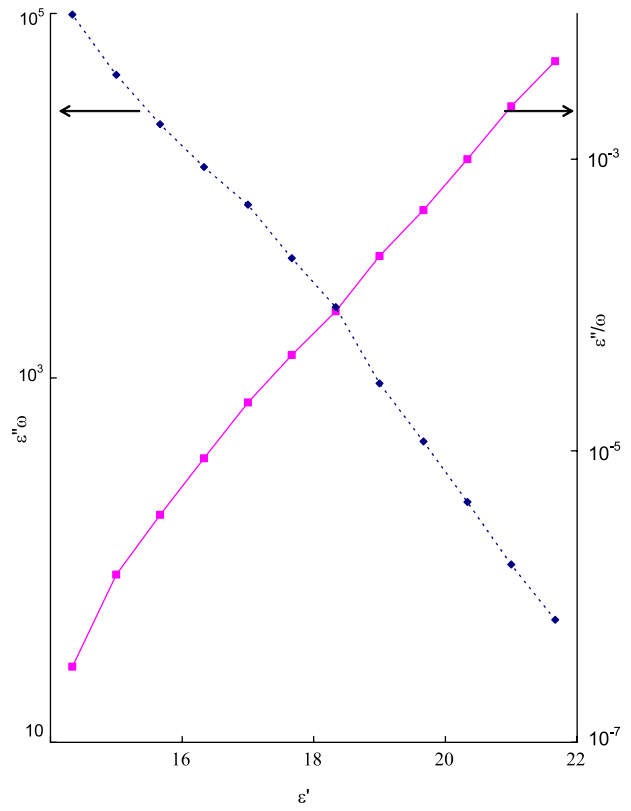

Figure 18. Variation of the quantities $\varepsilon''\omega$ and ε''/ω of glass ceramic C_{15} at 90 °C.

low temperature part of the conductivity (a near-temperature-independent part, as in the case of the present glass ceramics up to nearly 70 °C) can be explained on the basis of the quantum mechanical tunneling model as reported in a number of our earlier papers [39–41]. The analysis of the results of the dielectric properties also suggests that there is an increase in the dielectric breakdown strength (since it is inversely proportional to $\varepsilon' \tan\delta$) of these glass ceramics with increase in the content of CoO.

5. Conclusions

$PbO–Sb_2O_3–B_2O_3$ glasses have been crystallized with different concentrations of CoO. The scanning electron microscopic studies indicated that the samples contain well-defined and randomly distributed crystal grains. The x-ray diffraction studies indicated the formation of antimony cobalt oxide, antimony borate, lead antimony oxide and cobalt oxide crystalline phases. The study of DSC suggests the crystallization spreads from the inside to the surface of the samples as the concentration of CoO is increased. The IR and Raman spectral studies pointed out the presence of conventional BO_3, BO_4, SbO_3 and also Co^{III}–O vibrational groups in the glass ceramic samples. These studies have further indicated the decreasing concentration of symmetrical structural vibrational groups with increase in the concentration of CoO. The optical absorption and luminescence spectra of $PbO–Sb_2O_3–B_2O_3$ glass ceramics exhibit bands due to the transitions of tetragonally and octahedrally positioned Co^{2+} ions. In addition traces of Co^{3+} ions could also be located from these studies. These studies together with the result of magnetic susceptibility experiments have indicated that, with the increase in the concentration of the nucleating agent there is a gradual transformation of cobalt ions from tetragonal to octahedral coordination. The analysis of the results of dielectric studies suggests a decrease in the insulating character with increase in the crystallizing agent of these samples. The experiments on PIB indicated an increasing intensity of birefringence with increase in the concentration of CoO; simultaneously a redshift in the optical energy gap and a decrease in the crystal field strengths have been observed. This observation allows us to conclude that the surrounding ligands of octahedrally positioned cobalt ions play the principal role in the observed PIB.

Acknowledgment

Two of the authors (TS and NV) wish to thank the Defence Research and Development Organization, Government of India for the financial assistance of this work in the form of Major Research Project (grant no. ERIP/ER/0503545M/01/946).

References

[1] Esposito S, Turco M, Ramis G, Bagnasco G, Pernice P, Pagliuca C, Bevilacqua M and Aronne A 2007 *J. Solid State Chem.* **180** 3341–50
[2] Brik M G and Kityk I V 2007 *Solid State Commun.* **143** 326–30
[3] Duan X, Yuan D, Cheng X, Liu Z and Zhang X 2008 *J. Alloys Compounds* **453** 379–81
[4] Cattaruzza E, Battaglin G, Canton P, de Julian Fernandez C, Ferroni M, Finotto T, Maurizio C and Sada C 2004 *J. Non-Cryst. Solids* **336** 148–52
[5] Luo M, Jiang Y, Xu Ch, Yang X, Burger A and Giles N G 2006 *J. Phys. Chem. Solids* **67** 2596–602
[6] Abritta T and Black F H 1991 *J. Lumin.* **48/49** 558–60
[7] Camargo M B, Stultz R D, Birnbaum M and Kokta M 1995 *Opt. Lett.* **20** 339–41
[8] Uniyal A and Singh S P 2004 *Indian J. Pure Appl. Phys.* **63** 109–11
[9] Nalin M, Poulain M, Poulain M, Ribeiro S J L and Messaddeq Y 2001 *J. Non-Cryst. Solids* **284** 110–6
[10] Wang J S, Vogel E M and Snitzer E 1994 *Opt. Mater.* **3** 187–203
[11] Sabadel J C, Armand P, Cachau-Herreillat D, Baldeck P, Doclot O, Ibanez A and Philippot E 1997 *Solid State Chem.* **132** 411–9
[12] Mierczyk Z, Majchrowski A, Kityk I V and Gruhn W 2003 *Opt. Laser Technol.* **35** 169–72
[13] Srinivasa Rao L, Srinivasa Reddy M, Krishna Rao D and Veeraiah N 2009 *J. Solid State Sci.* **11** 578–87
[14] Sambasiva Rao K, Srinivasa Reddy M, Ravi Kumar V and Veeraiah N 2008 *Mater. Chem. Phys.* **111** 283–92
[15] Powder Diffraction File *Alphabetical Index, Inorganic Compounds* 2003 (Newtown Square, PA: JCPDS—International Centre for Diffraction Data)
[16] Rao K J 2002 *Structural Chemistry of Glasses* (Amsterdam: Elsevier)
[17] Srinivasarao G and Veeraiah N 2002 *J. Solid State Chem.* **166** 104–17

[18] Rao K J, Benqlilou-Moudden H, Desbat B, Vinatier P and Levasseur A 2002 *J. Solid State Chem.* **165** 42–7
[19] Maniu D, Iliescu T, Ardelean I, Bratu I and Dem C 2001 *Stud. Univ. Babes-Bolyai Physica* special issue 366–71
[20] Beattie I R, Livingston K M S, Ozin G A and Reynolds D J 1970 *J. Chem. Soc.* A 449–51
[21] Kotkova K, Ticha H and Tichy L 2008 *J. Raman Spectrosc.* **39** 1219–26
[22] Chryssikos G D, Bitsis M S, Kapoutsis J A and Kamitsos E I 1997 *J. Non-Cryst. Solids* **217** 278–90
[23] Zahra A M, Zahra C Y and Piriou B 1993 *J. Non-Cryst. Solids* **155** 45–55
[24] Dubois B, Videau J J and Portier J 1986 *J. Non-Cryst. Solids* **88** 355–65
[25] Miller P J and Cody C A 1982 *Spectrochim. Acta* A **38** 555–9
[26] Raghavaiah B V and Veeraiah N 2003 *Phys. Status Solidi* a **199** 389–402
[27] Holland D, Hannon A C, Smith M E, Johnson C E, Thomas M F and Beesley A M 2004 *Solid State Nucl. Magn. Reson.* **64** 172–9
[28] Damodaran K V and Rao K J 1988 *Chem. Phys. Lett.* **148** 57–61
[29] Srinivasa Reddy M, Sridhar Raja V L N and Veeraiah N 2007 *Eur. Phys. J. Appl. Phys.* **37** 203–11
[30] Greenwood N N and Earnshaw A 1997 *Chemistry of the Elements* 2nd edn (Oxford: Butterworth-Heinemann)
[31] Tanaka K 1985 *Solid State Commun.* **54** 867–79
[32] Marotta A, Buri A and Branda F 1981 *J. Mater. Sci.* **16** 341–4
[33] Kuleshov N V, Mikhailov V P, Scherbitsky V G, Prokoshin P V and Yumashev K V 1993 *J. Lumin.* **55** 265–9
[34] Wood D L and Remeika J P 1967 *J. Chem. Phys.* **46** 3595–602
[35] Duan X, Yuan D, Cheng X, Sun Z, Sun H, Xu D and Lv M 2003 *J. Phys. Chem. Solids* **64** 1021–5
[36] Ryba-Romanowski W, Golab S, Dominiak-Dzik G and Berkowski M 1999 *J. Alloys Compounds* **288** 262–8
[37] Ferguson J, Wood D L and Van Uitert L G 1969 *J. Chem. Phys.* **51** 2904–10
[38] Ardelean I, Ilonca Gh, Simin V, Barbur I, Filip S and Jurcut T 1999 *J. Magn. Magn. Mater.* **196** 255–6
[39] Kojima K, Taguchi H and Matsuda J 1991 *J. Phys. Chem.* **95** 7595–8
[40] Belkhouaja M, Et-Tabirou M and Elmoudane M 2003 *Phase Transit.* **76** 645–52
[41] Sahaya Baskaran G, Krishna Rao D and Veeraiah N 2008 *Solid State Commun.* **145** 401–6
[42] Sankarappa T, Prashant Kumar M, Devidas G B, Nagaraja N and Ramakrishnareddy R 2008 *J. Mol. Struct.* **889** 308–15
[43] Murali Krishna G, Anila Kumari B, Srinivasa Reddy M and Veeraiah N 2007 *J. Solid State Chem.* **180** 2747–55
[44] Kumar V R, Veeraiah N and Buddudu S 1997 *J. Physique* III **7** 951–61
[45] Bottcher C J F and Bordewijk P 1978 *Theory of Electric Polarization* (Amsterdam: Elsevier)
[46] Elliott S R 1990 *Physics of Amorphous Materials* (Essex: Longman)